Journal of Power Sources 201 (2012) 340–346

Contents lists available at SciVerse ScienceDirect

Journal of Power Sources

journal homepage: www.elsevier.com/locate/jpowsour

A cost-effective way to maintain metal-doped carbon xerogels and their applications on electric double-layer capacitors

Xin Lu, Jianfeng Shen, Hongwei Ma, Bo Yan, Zhiqiang Li, Min Shi, Mingxin Ye*

Center of Special Materials and Technology, Fudan University, 220 Handan road, Shanghai 200433, China

ARTICLE INFO

Article history:
Received 29 July 2011
Received in revised form 24 October 2011
Accepted 31 October 2011
Available online 4 November 2011

Keywords:
Metal-doped carbon xerogel
Catalytic graphitization
2 Dimensional channel-like nanostructure
3 Dimensional connective mesoporous structure
Electric double-layer capacitor
Electrochemical properties

ABSTRACT

Metal-doped carbon xerogels (M-DCXs, M = Co, Fe, and Ni) have been obtained by a cost-effective sol–gel method using metal nitrates as catalyst, followed by solvent exchange and then dried in ambient conditions before carbonization procedure. It is found that the existence of metals could also lead to 2 dimensional (2D) channel-like nanostructure caused by layered deposits of graphite during the carbonization procedure. The performance of M-DCXs for electric double-layer capacitors is proved to be associated with their nanostructure. As a result, the as-prepared Co-DCX can make full use of the 2D channel-like nanostructure of ordered graphite and 3D connectivity of mesoporous structure of carbon xerogel, and thus, exhibits the highest capacitance of 84 F g^{-1}. At the same time, Co-DCX also shows a stable long-term cycling behavior with less than 2% loss of capacitance after 2000 cycles.

1. Introduction

The ever worsening energy depletion and global warming issues call for not only urgent development of clean alternative energies and emission control of global warming gases, but also more advanced energy storage and management devices [1]. Electrochemical supercapacitors, which are one of the most promising electrochemical energy storage systems, have attracted considerable attention since they can provide higher power densities and have a longer cycle life than batteries [2–4]. Electrochemical supercapacitors store charge at a polarized solid/electrolyte interface and, consequently, their capacity depends on the available surface area of the porous materials accessible to the electrolyte. The porous electrodes of supercapacitors may consist of metal oxides obtained mainly from sol–gel polymerization of transition metal alkoxides and functionalized with ferrocene derivatives [5–10]. Due to the properties of ultrahigh specific surface area, controllable pore size distribution and low resistivity, carbon gels (CGs) could be an excellent candidate for electrode materials of electrochemical supercapacitors.

The earliest CG been reported is carbon aerogel (CA) and the key to the production of low density aerogels was firstly proposed by Kistler in 1931, applying "supercritical drying" of gels [11,12]. Chemistry of aerogel synthesis was then further developed starting from the 1960s [13,14]. Currently, the general method to prepare CA follows Pekala's: polymerization of resorcinol and formaldehyde, with sodium carbonate as catalyst to get organic aerogel (OA), and then treat OA with supercritical drying, ultimately CA formed after the carbonization of dried OA. CA prepared in this method showed a capacitance of 95 F g^{-1} [15]. However, this method by Pekala is of high energy consumption and supercritical drying technology also increases the cost of CA preparation, which would limit the practical applications of CA. As the result, innovation of the general drying method is much more necessary. In recent years, drying methods like ambient pressure drying [16], freeze drying [17], microwave drying [18] were tried. Of these drying methods, ambient pressure drying after solvent exchange is the most cost-effective one, and xerogels are defined as the gels prepared instead of aerogels.

Nevertheless, the possibility that CGs be applied to supercapacitors is also limited to its electrical properties. Many charge–storage mechanisms have been proposed for supercapacitors, while electric double-layer (EDL) capacitance and charge-transfer-reaction pseudocapacitance are mostly accepted [19,20]. EDL capacitance arises from the potential difference at the interface between a solid electrode and an electrolyte [6,20], whereas pseudocapacitance arises from fast, reversible faradic reactions occurring at or near a solid electrode surface over an appropriate range of potential [21–23]. So far, activate carbon material with a specific surface area up to 3000 m^2 g^{-1} have been found [24]. However, its actual utilization

* Corresponding author. Tel.: +86 021 55664095; fax: +86 021 55664094.
E-mail address: mxye@fudan.edu.cn (M. Ye).

0378-7753/$ – see front matter © 2011 Elsevier B.V. All rights reserved.
doi:10.1016/j.jpowsour.2011.10.099

is about 10%. In order to get CGs for EDL capacitors, a mixture of 2 dimensional (2D) active graphitic structure and 3D connectivity of mesoporous structure was reported to be much more suitable [25]. Moreover, pore size distribution also plays a key role in the determination of the EDL capacitance. Three factors affect the EDL capacitance: specific surface area, pore accessibility by ions and EDL formation. Due to an overall decrease in the specific surface area, the occurrence of mesopores may reduce the EDL capacitance. In contrast, most of the specific surface area is derived from microporous surface area and those micropores show a slow charging process and cause a substantial loss of EDL capacitance. The diffuse layer of micropores plays an essential part in the EDL capacitance in low electrolyte concentrations or low electric fields. Double-layer overlapping can be reduced by increasing the pore size, electrolyte concentration and electric field. As a result, a balanced surface area ratio of micropores to mesopores is necessary for an effective EDL capacitor under various operating conditions of electrolyte concentration and applied potential [26]. It is now known that, suitable pore sizes, 2–5 nm, of the porous electrode materials are critical to ease the mass transfer of electrolytes within the pores for fast redox reactions and EDL charging/discharging [27–30].

While conventional activating procedures usually used to prepare activated carbons with high surface area, which would present the creation of pores, are no longer suitable for gasifying agents. To form well-developed graphitic structure, the heat treatment temperature of porous carbon should be higher than 2000 °C, but such reaction conditions are costly. Additionally, the extremely high temperature may also result in decrease of the surface area and pore volume of the porous carbon [31]. To solve these problems, transition metals have been introduced to catalyze the graphitization of amorphous carbon, which can lower the carbonization temperature and result in metal-doped carbon gels (M-DCGs). Many groups have been working on this area. For example, Wang et al. [32] have developed an easy co-gelation sol–gel route for the synthesis of porous graphitic carbons by using three kinds of precursors, including tetraethylorthosilicate, furfuryl alcohol and $Co(NO_3)_2$. After that, the samples were pyrolyzed at 900 °C and treated with 48% HF solution. Such graphitic porous carbons were successfully applied to supercapacitors and exhibited good capacitive performances with high-rate response and low electronic resistance. Fu et al. [33] presented the synthesis and characterization of Co- and Ni-DCGs prepared by ion exchange method, with the carbonization temperature of 1050 °C, finding that carbonization of these M-DCGs would result in the formation of metal nanoparticles as well as the growth of carbon nanostructures within the CG framework. Furthermore, they have studied the growth of carbon nanostructure on Co-DCG by carbonizing its corresponding precursor directly at various temperatures [34]. Unfortunately, these synthetic processes mentioned above are so time-consuming or complex that they are not suitable for large-scale practical applications.

Recently, CGs prepared by ambient pressure drying were reported with a relatively low EDL capacitance. Kim et al. reported that carbon xerogel (CX) electrode pyrolyzed at 1073 K showed the specific capacitances of about 40 F g^{-1} in H_2SO_4 electrolyte solution and 35 F g^{-1} in KOH solution [35]. Furthermore, with the application to capacitor devices, long-term cycling behavior of those CGs is also particularly important. However, it seems difficult to improve the cycling behavior, while the loss rate of capacitance after 2000 cycles was reported about 10% [1,36]. For this reason, a new method to synthesis M-DCGs with a higher capacitance and more stable long-term cycling behavior seems significant.

In this work, we developed an easy sol–gel route for the synthesis of porous graphitic carbon xerogels. In the early days, Lee et al. [37] have reported that cobalt was impregnated onto CA after a resorcinol/formaldehyde (RF) method to prepare Co-DCG. Based on it, we have tried a sol–gel route in which there is a mixture of metal nitrates, resorcinol and formaldehyde. Metal nitrates were used instead of the traditional catalyst sodium carbonate. After that, metals can catalyze the formation of the graphitic carbon in a relatively low temperature, and thus a mixture of 2D active graphitic structure and 3D connectivity of mesoporous structure was formed. In this way, metal nitrates played both the role of catalyst of sol–gel reaction and metal precursors, and various metal-doped carbon xerogels (M-DCXs, M = Co, Ni, and Fe) were prepared. Moreover, the physical properties and electrochemical performances of the as prepared Co-DCX show that it is an excellent material for EDL capacitors.

2. Experimental

2.1. Preparation of CX and M-DCXs

Resorcinol, formaldehyde and metal nitrates were all supplied by Shanghai Chemical Reagent Company. They were of analytical reagent grade and used without further purification.

Different samples were prepared by a sol–gel route of metal nitrates, resorcinol and formaldehyde at 70 °C, followed by solvent exchange and then dried in ambient condition. After that, a carbonization treatment was further taken under nitrogen atmosphere. In a typical run, 0.02 mol resorcinol and 2 mmol metal nitrates were dissolved in 2 mL distilled water, followed by addition of 0.04 mol formaldehyde. The solution took 72 h at 70 °C in a water bath for the sol–gel process and dark red gels were obtained. Afterwards, samples were immersed twice in acetone for solvent exchange, each for 12 h. All samples were dried in ambient condition and carbonized under nitrogen atmosphere, with a heating rate of 5 °C min^{-1} to 950 °C, and then kept at 950 °C for another 2 h. The final products were denoted as M-DCXs, while M is corresponding to the metal precursor used in the synthesis route.

The same procedure was carried out to prepare the sample of CX, except that 0.04 mmol sodium carbonate was used instead of metal nitrates.

2.2. Preparation of CX electrode and M-DCXs electrode

The prepared CX and M-DCXs were cast into electrode using acetylene black and polyvinylidene fluoride (PVDF) as a conductive additive and a binder, respectively, with weight ratio of 75:15:10. The binder was further dispersed in N-methyl-2-pyrrolidone (NMP), after which the mixture was then coated onto nickel mesh and dried. The obtained electrode showed an area of 1 cm^2 and a thickness of 200 μm. The weight of binder on each electrode was about 15 mg. Before electrical measurements, those electrodes were infiltrated in 6 M KOH electrolyte for 30 min at vacuum condition.

2.3. Characterization

Thermogravimetric analysis (TGA) was conducted with Netzsch TG 209F1 that was fitted to an air purge gas at 5 °C min^{-1} heating rate. Wide-angle X-ray diffraction (XRD) was taken on D/max-rB diffractometer using Cu Kα radiation. Raman spectra were recorded on a Dilor LABRAM-1B multi-1B multi-channel confocal microspectrometer with 514 nm laser excitation. N_2 adsorption–desorption isotherms were measured with Micromeritics 2020 analyzer at 77 K. Before measurements, the samples were degassed at 150 °C for 5 h. The specific surface areas were calculated in Brunauer–Emmett–Teller (BET) method. The pore size distributions were derived from the adsorption branches of the isotherms based on the Barrett–Joyner–Halanda (BJH) model. The total pore

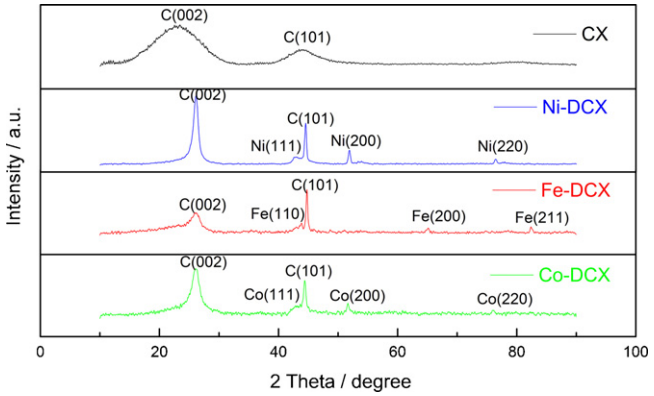

Fig. 1. Powder XRD patterns for CX and M-DCXs.

volume was estimated from the amount absorbed at a relative pressure (P/P_0) of 0.99.

2.4. Electrochemical measurement

Electrochemical properties of CX and M-DCXs electrodes were measured with a conventional three-electrode cell system in 6 M KOH electrolyte. A platinum plate and Ag/AgCl were selected as a counter electrode and a reference electrode, respectively. The electrochemical performance of the CX and M-DCXs electrodes were conducted to evaluate by cyclic voltammograms measurements at a scan rate of 1, 10, 50, 100 mV s^{-1} within voltage range from −0.5 to −1 V to avoid the apparent oxygen-evolution reaction and the oxidation reactions of metals. Galvanostatic charge/discharge measurements and long-term cycling behavior were carried out at a constant current of 1 A g^{-1} within voltage range from −0.5 to −1 V.

3. Results and discussion

One purpose of this study is to find a cost-effective way to prepare M-DCGs for EDL capacitors. Generally, sodium carbonate was used as catalyst in the sol–gel reaction, followed by metal impregnation to prepare M-DCGs. It would be interesting if these two steps could combine into one, which is adding metal precursors directly in the sol–gel procedure, playing the role of catalyst. However, these attempts have rarely been reported, for some alkaline substances, such as Na_2CO_3 and $Ca(OH)_2$, were recognized as the common catalyst for the preparation of CG and M-DCGs. As Co, Ni and Fe were reported to catalyze the graphitization of CG [5], their nitrates were used in this work. To obtain the ideal porous properties, especially pore size distribution, it's much necessary to control the ratio of reactants. Usually, in preparation of CGs, different molar ratios of resorcinol and catalyst to control the crosslinking degree can be used to form various texture structure. A higher ratio of resorcinol and catalyst will result in a larger pore aperture and a smaller specific surface area [38]. Here, we found that an amount of 2 mmol metal nitrates is appropriate. Additionally, the unequal amount of 0.04 mmol sodium carbonate used in the preparation of CG was reported to form the pore distribution of 2–5 nm in aperture [39].

XRD patterns of the different M-DCXs and CX samples are shown in Fig. 1. The two broad diffraction peaks of CX pattern at about 23.5° and 43° were attributed to a largely amorphous structure of the carbonaceous matrix, respectively. While for samples of M-DCXs, the broad bands corresponding to the carbonaceous matrix became narrower, with higher intensity. Moreover, the diffraction angles were now around 26° and 44.5°, corresponding to the (0 0 2) and (1 0 1) diffraction peaks of graphitic framework, respectively, according to the JCPDS card number 41-1487. Compared to carbonaceous matrix, the two peaks of M-DCXs shifted toward the high angle, suggesting that the interlayer distance between the carbonaceous matrix planes was slightly larger than normal graphite [40]. Together with these graphitic framework, the XRD diffraction peaks corresponding to metal species also appeared (for example, peaks at 44, 65.2 and 82.5° presented for Fe), indicating the successful impregnation of metal species on CX.

Table 1
Characteristics of the stack height (L_c) of CX and different M-DCXs microcrystallites.

Sample	θ (°)	B (°)	L_c (nm)
CX	23.41	8.64	0.99
Ni-DCX	26.11	0.99	8.8
Fe-DCX	25.92	2.45	3.6
Co-DCX	26.01	1.70	5.1

Moreover, we can calculate the crystallite sizes of graphite perpendicular to the basal plane (L_c) from the (0 0 2) reflections, using Scherrer formula:

$$L_c = \frac{0.89\lambda}{B\cos\theta} \quad (1)$$

where λ is the wavelength of the X-ray (1.54 Å), B is the full angular width at half max, and θ is the Bragg's angle. The monotonic increase in the values of L_c (Table 1) shows progressive graphitization of the carbon, and from which we can easily find the graphitization degree as follows: Ni-DCX > Co-DCX > Fe-DCX > CX.

It seems to work in theory that the in-plane width of graphitic layers, L_a, could be calculated from the (1 0 1) diffraction peak. However, as we can see in the XRD patterns, this (1 0 1) peak was very near to or even overlapped by the maximum intensity peak of the metal phases, and consequently, was not appropriate to determine this parameter. Instead, Raman spectra would do.

Raman spectra of CX and M-DCXs are shown in Fig. 2. For all four samples, there were two apparent peaks in the spectra between the frequency shift of 1000 cm^{-1} and 2000 cm^{-1}. As was first reported by Tuinstra and Koening [40], a band around 1350 cm^{-1} (called D-band) is associated with the disorder-induced scattering produced by imperfections or loss of hexagonal symmetry in the carbon structure which is attributed to the A_{1g} mode [41] and does not appear in perfect graphite crystals. While another band around 1580 cm^{-1} (called G-band) is assigned to the Raman active $2E_{2g}$ vibration mode in 2D network structure, which always appears in all carbon and graphite materials. By determining the area under the peak of D band and G band, the ratio of amorphous to graphitic carbon was presented by R ($R = I_D/I_G$). The decreasing of R indicates the improving degree of graphitization with the catalytic effect of the metals. At the same time, the half-width of both bands were lowered by the addition of metals (Table 2). Tuinstra and Koening [40] also reported a linear relationship between the inverse of the in-plane

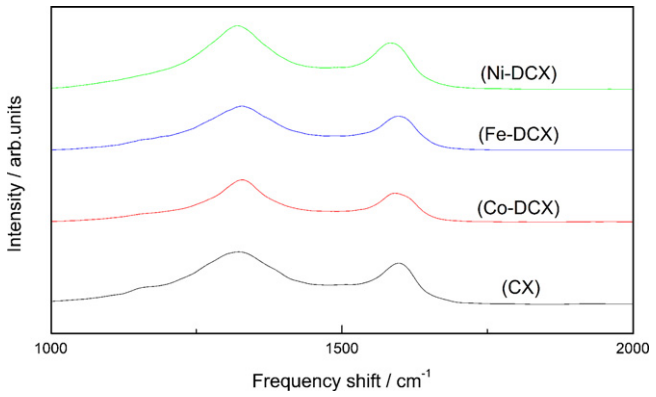

Fig. 2. Raman spectra for CX and different M-DCXs.

Table 2
Characteristics of the D and G Raman bands and in-plane width of the graphite microcrystallites.

Sample	Band width		Relative intensity $R = I_D/I_G$	L_a (nm)
	ΔD (cm^{-1})	ΔG (cm^{-1})		
CX	188.6	108.6	2.26	1.95
Co-DCX	118.5	84.94	1.91	2.30
Fe-DCX	152.1	102.8	1.97	2.23
Ni-DCX	158.0	90.87	2.10	2.10

width of the graphene layers, L_a, and the relative integrated intensity ratio, R, which was stated L_a (nm) = 4.4/R. The data obtained are also shown in Table 2. L_a increases while R decreases, indicating the growth in size of graphitic crystallites with the addition of metal as catalyst.

TGA analysis of M-DCXs was performed to find out different metal content in these samples. Fig. 3 shows the TGA profiles of M-DCXs measured in air conditions. The residual weight percentages were 0%, 8.0%, 10.1%, and 8.8% for CX, Co-DCX, Fe-DCX and Ni-DCX, respectively. As the residues were metal oxides, the metal content of each sample was calculated to be 0%, 6.3%, 7.1% and 6.9%, respectively. The residual mass percentages of M-DCXs were very close, indicating this method is reliable in preparation of samples with a certain ratio of metals. Moreover, as seen in the TGA curves, Fe-DCX and Ni-DCX had a higher starting decomposition temperature than CX, for graphitized carbons with higher graphitization degree were more stable against air oxidation. While cobalt oxide was reported as a catalyst of the oxidation of carbon [42], the starting decomposition temperature of Co-DCX was close to that of CX and the range of decomposition temperature was much narrower. The influence of different metals and graphitization degrees to the pore structure was further surveyed by the N_2 adsorption/desorption tests.

The nanostructure characteristics of the CX and M-DCXs were investigated with the N_2-adsorption/desorption isotherms and pore distribution, which are shown in Figs. 4 and 5. Important structural parameters were derived from the isotherms and tabulated in Table 3. All these samples showed type IV isotherms with a distinct hysteresis loop, indicating typical mesoporous structure characteristic. As seen in Fig. 4, CX exhibited a type H2 hysteresis loop, which showed the "ink bottle" liked pores caused by uniform particle packing, while M-DCXs presented a mixture of type H3 and H4 hysteresis loops, indicating the 2D channel-like porous structure caused by layered deposits of graphite. Compared with CX, the decreasing in the specific surface area of M-DCXs was due to

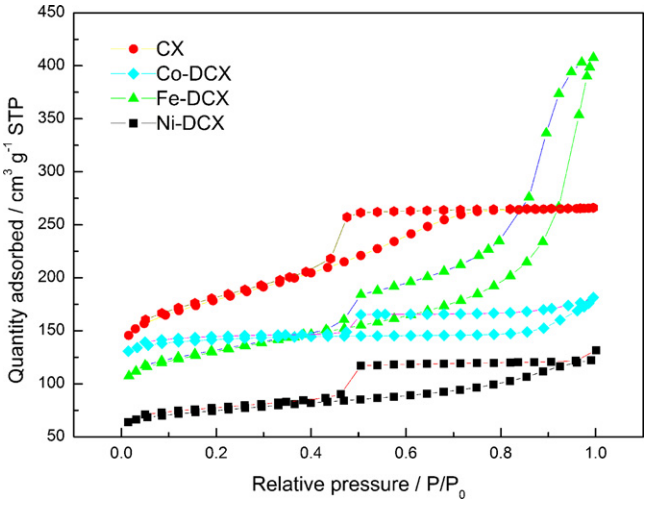

Fig. 4. N_2 adsorption/desorption isotherms of CX and M-DCXs.

their high graphitization degree, which would result in breakage of porous structure. Furthermore, the particularly high graphitization degree of Ni-DCX leaded to a much less specific surface area among all samples.

The BJH pore size distribution plots, determined from the adsorption branch of the N_2 isotherms, presented a majority between 2 nm and 5 nm of diameter. While for Fe-DCX, another wide pore distribution around 16.5 nm appeared. This was in accordance with the performance of N_2-adsorption/desorption isotherm. It may also due to the catalytic effect of Fe in the heat treatment at high temperature, leading to the even more shrinkage of the 3D microporosity of the sample, which resulted in the increasing of pore volume and a shift of the pore size distribution to larger size [5].

Cyclic voltammograms at different scan rate for CX and M-DCXs samples are given in Fig. 6, respectively. No any oxidation or reduction peaks were observed in all samples, means only double-layer capacitance exists in these samples. Meanwhile, it is well known that an ideal nanostructure for EDL capacitors should be capable of providing very fast ion transport pathways, thus the EDL can be re-organized quickly at the switching potentials, resulting in a rectangular-shaped CV curve [43]. The rectangle degree of CV curve can reflect the ion diffusion rate within a carbon nanostructure. It can be found that with the increasing of scan rate, the

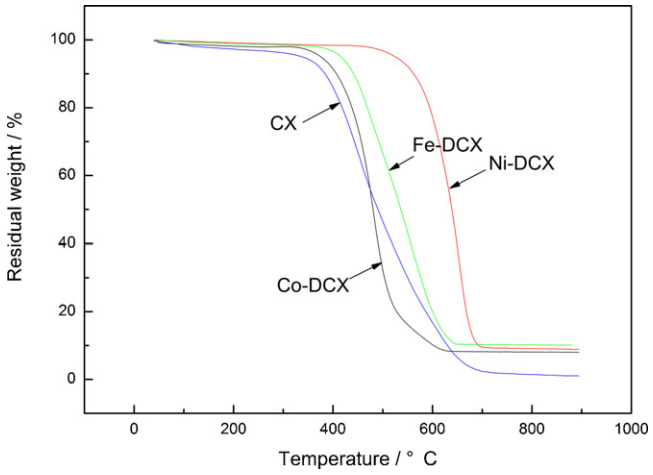

Fig. 3. TGA curves of CX and different M-DCXs.

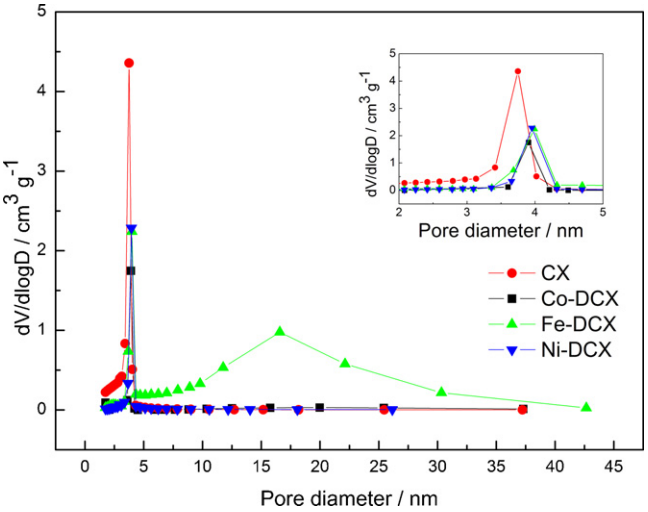

Fig. 5. BJH pore size distribution of CX and M-DCXs.

Table 3
Structural parameters of CX and M-DCXs.

Sample	BET surface area ($m^2\ g^{-1}$)	Micropore surface area ($m^2\ g^{-1}$)	Mesopore surface area ($m^2\ g^{-1}$)	BJH pore volume ($cm^3\ g^{-1}$)	Micropore volume ($cm^3\ g^{-1}$)	Mesopore volume ($cm^3\ g^{-1}$)	Average pore diameter (nm)	Pore distribution (nm)
CX	621	319	302	0.412	0.145	0.267	3.45	3.75
Co-DCX	482	358	124	0.280	0.109	0.171	4.70	3.90
Fe-DCX	451	271	180	0.631	0.124	0.507	8.27	3.99, 16.5
Ni-DCX	257	180	77	0.204	0.082	0.122	3.90	3.95

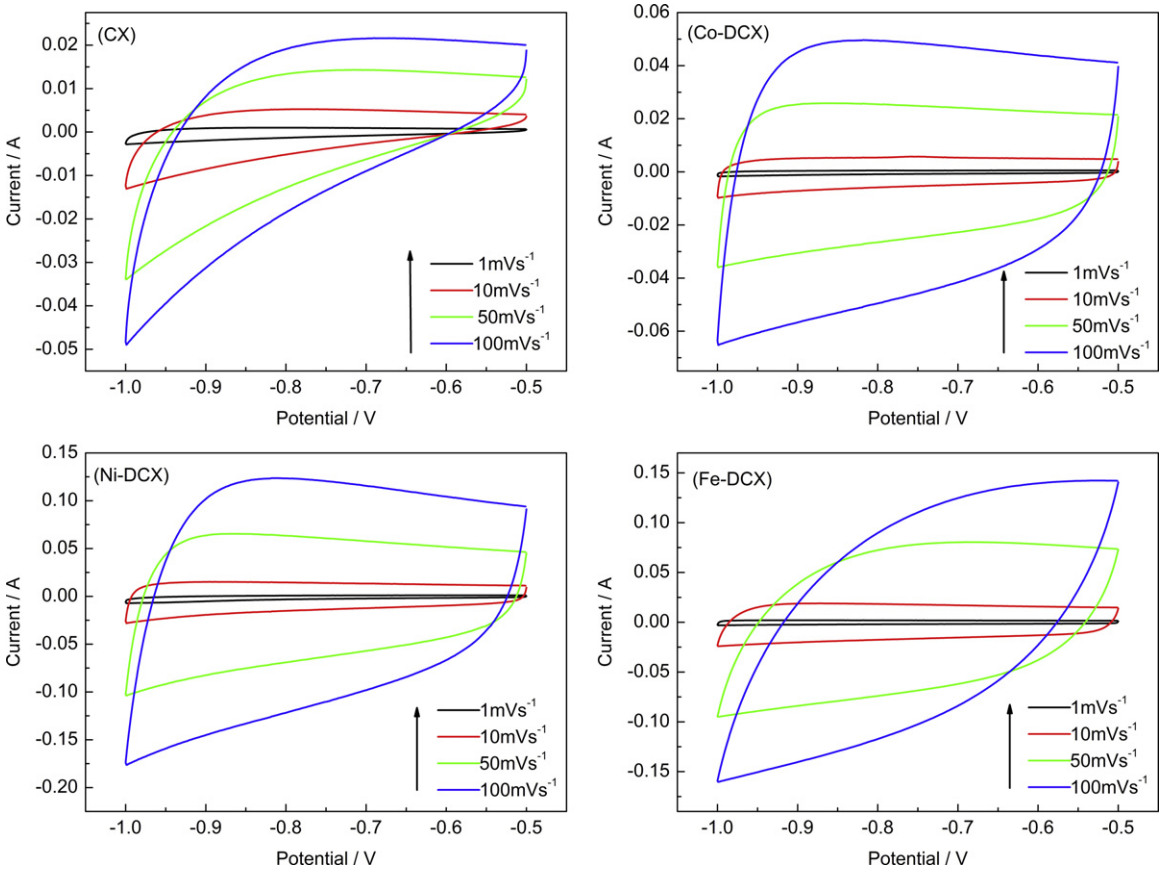

Fig. 6. Cyclic voltammograms at 1, 10, 50, and 100 mV s^{-1} of scan rate for CX and different M-DCXs.

CX sample gave a poorer rectangular-shaped CV curve, indicating that the nanostructure of CX is inconvenient for ion diffusion. This can be explained with the "ink bottle" liked porous structure caused by uniform particle packing shown in the N_2 adsorption/desorption isotherms, which is accompanied with the uneven distribution of the pore diameter. At the same time, both Co-DCX and Ni-DCX exhibited good rectangular-shaped CV curves, showing that the 2D channel-like active graphitic structure formed by the layered deposits of graphite were able to provide fast ion transport pathways at a wide range of scan rate. While the shrinkage of the 3D microporosity of Fe-DCX may lead to blockades among those 2D channels, it may result in the decrease of the rectangle degree of CV curves at a higher scan rate.

To analyze the variation of capacitance under different scan rate, the CV measurement was carried out, and the specific capacitance of the electrode can be calculated by the equation:

$$C = \frac{Q}{V} = \frac{\int idt}{\Delta V} \quad (2)$$

where i is a sampled current, dt is a sampling time span, and ΔV is the total potential deviation of the voltage window. Fig. 7 shows the specific capacitance variations of CX and M-DCXs with scan rate

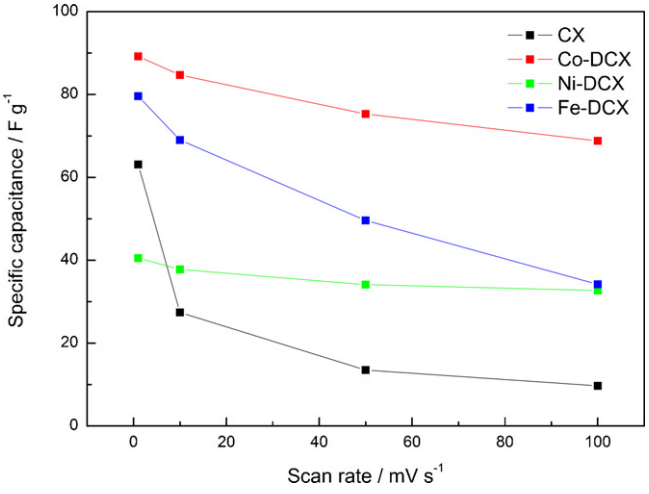

Fig. 7. Specific capacitance of CX and M-DCXs at different scan rate.

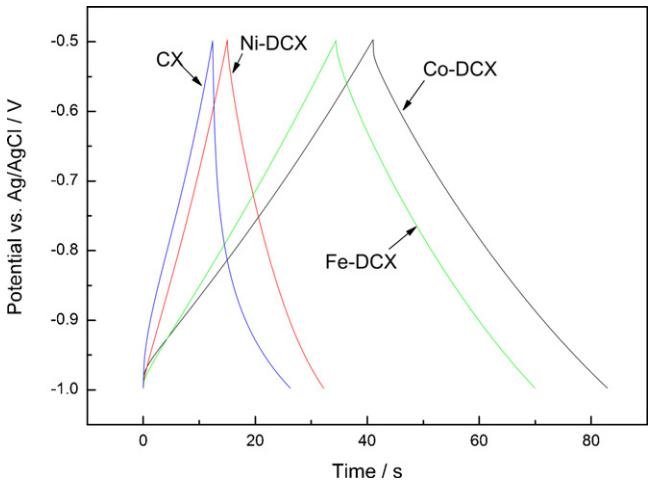

Fig. 8. Charge/discharge curves of CX and M-DCXs.

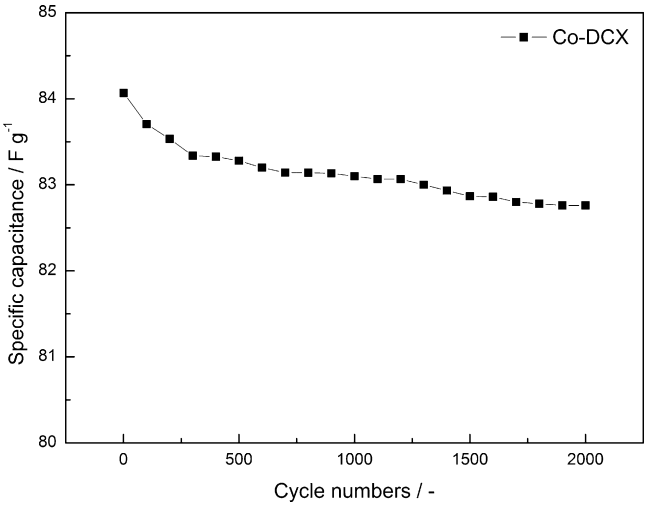

Fig. 9. Long-term cycling behavior of Co-DCX.

from 1 mV s^{-1} to 100 mV s^{-1}. The retained ratios of CX, Co-DCX, Ni-DCX and Fe-DCX were as 15%, 77%, 81% and 43%, respectively, and Co-DCX had a higher specific capacitance at all scan rate than other samples. These can be interpreted in two aspects: the fast ion transport pathways contributed by the 2D active graphitic channels and the ability of micropores to store charge [44]. Moreover, these results highlighted the suitability of Co-DCX and Ni-DCX for high-rate operation. As we described above, a balanced surface area ratio of micropores to mesopores is necessary for an effective EDL capacitor under various operating conditions. Co-DCX and Ni-DCX showed higher microporosities than others, from which we believe that a relatively higher microporosities is beneficial.

Fig. 8 shows the charge/discharge behaviors of CX and M-DCXs at constant current (1 A g^{-1}), and the calculated specific capacitances are summarized in Table 4. The specific capacitances were calculated from the following equation.

$$c = \frac{I\Delta t}{m\Delta V} \tag{3}$$

Here, I is the discharge current, Δt is the discharge time, m is the mass of an active material, and ΔV is the potential change during discharging.

From these curves, large inner resistance (IR) drop intensity of CX was clearly observed, while others' were negligible. This potential drop was attributed to the resistance of electrolyte and the inner resistance of ion diffusion in carbon micropores. It is noteworthy that Co-DCX electrode showed the highest specific capacitance among the M-DCXs, which is well consistent with the results of specific capacitances measurement by cyclic voltammograms.

In general, EDL capacitance increases with the available surface area. For pure graphite surface, the EDL capacitance per unit volume is about 20 μF m^{-2} [45]. Although Ni-DCX had the highest degree of crystallinity, its available surface area was much less than others', which leaded to the lower capacitance. While due to its discontinuous 3D network conducted by lacking of sp^2-bonded carbon, CX could not make full use of its highest specific surface area [46]. The specific capacitance of Co-DCX was superior to others for its relatively high specific surface area, well constructed 2D channel-like porous structure and the appropriate surface area ratio of micropores to mesopores caused by the graphitization process, which was suitable for ion diffusion.

Moreover, the cycle life is another important factor for the EDL capacitors. Fig. 9 shows the cycling behavior of Co-DCX electrode. The cycle life curve of the sample was measured at the current density of 1 A g^{-1}. From Fig. 9, the specific capacitance of Co-DCX EDL capacitors reached around 83 F g^{-1}, and the loss of capacitance was apparently low. After 2000 cycles, the capacitance dropped from 84.1 F g^{-1} to 82.7 F g^{-1}, with a loss rate less than 2%. Hence, the Co-DCX composites had better long-term cycle life for electrical devices. The excellent cycle stability of Co-DCX was due to its firm porous structure during the long-term cycling behavior.

Table 4
Specific capacitance of CX and M-DCXs calculated by charge/discharge measurements.

Samples	CX	Co-DCX	Ni-DCX	Fe-DCX
Specific capacitance (F g^{-1})	26	84	37	70

4. Conclusions

In summary, the porous M-DCXs were successfully fabricated by a simple sol–gel method. By this process, CX with uniformly dispersed metal ions was formed during the polymerization of resorcinol and formaldehyde with metal nitrates as catalyst of the sol–gel reaction. After which, metals also acted the role of catalyst in the carbonization process of organic gels. This synthesis process was much simpler in comparison with the conventional preparation methods. Based upon the experimental results, it can be found that the addition of metal can catalyze the formation of 2D channel-like nanostructure which showed an obvious complementary effect on ion diffusion properties. And thereby the 2D channel-like nanostructure would improve the utilization rate of the surface for charge storage, especially in the case of rapid charge/discharge operations. Furthermore, the experiments also provided useful information to determine the appropriate surface area ratio of micropores to mesopores for the use of EDL capacitors.

As a result, Co-DCX exhibited excellent electrical properties, not only in the specific capacitance measured at different scan rate, but also the long-term cycle stability. The existence of Ni could bring about a considerably high graphitization degree, which results in a substantially decrease in the specific surface area and the specific capacitance. For Fe-DCX, the even more shrinkage of the microporosity would block up the connection among the inner 2D channel-like active graphitic structure, and the limitation of ion diffusion also affected the specific capacitance of Fe-DCX electrode. Furthermore, this synthetic method of M-DCXs for EDL capacitors is expected to be applicable for other metals of technological importance.

References

[1] T.Y. Wei, C.H. Chen, H.C. Chien, S.Y. Lu, C.C. Hu, Adv. Mater. 22 (2010) 347.
[2] R.W. Pekela, J. Mater. Sci. 24 (1989) 3221.
[3] R.W. Pekala, C.T. Alviso, F.M. Kong, S.S. Hulsey, J. Non-cryst. Solids 145 (1992) 90.
[4] F.M. Kong, J.D. LeMay, S.S. Hulsey, C.T. Alviso, R.W. Pekala, J. Mater. Sci. 8 (1993) 3100.
[5] F.J. Maldonado-Hódar, C. Moreno-Castilla, J. Rivera-Utrilla, Y. Hanzawa, Y. Yamada, Langmuir 16 (2000) 4367.
[6] S. Sarangapani, P. Lessner, J. Forchione, A. Griffith, A.B. Laconti, J. Power Sources 29 (1990) 355.
[7] P. Audebert, C. Demaille, C. Sanchez, Chem. Mater. 5 (1993) 911.
[8] P. Audebert, P. Calas, G. Cerveau, R. Corriu, N. Costa, J. Electroanal. Chem. 372 (1994) 275.
[9] H. Cattey, P. Audebert, C. Sanchez, New J. Chem. 20 (1996) 1023.
[10] H. Cattey, P. Audebert, C. Sanchez, P. Hapiot, J. Phys. Chem. B 102 (1998) 911.
[11] S.S. Kistler, Nature 127 (1931) 741.
[12] S.S. Kistler, J. Phys. Chem. 34 (1932) 52.
[13] H.D. Gesser, P.C. Goswami, Chem. Rev. 89 (1989) 765.
[14] N. Hüsing, U. Schubert, Angew. Chem. Int. Ed. 22 (1998) 37.
[15] J.S. Huang, B.G. Sumpter, V. Meunier, Chem. Eng. J. 14 (2008) 6614.
[16] D.C. Wu, R.W. Fu, J. Porous Mater. 15 (2008) 29.
[17] H. Tamon, H. Ishizaka, T. Yamamoto, Carbon 37 (1999) 2049.
[18] L. Zubizarreta, A. Arenillas, J.A. Menéndez, J.J. Pis, J.P. Pirard, N. Job, J. Non-Cryst. Solids 354 (2008) 4024.
[19] J.P. Zheng, J. Huang, T.R. Jow, J. Electrochem. Soc. 144 (1997) 2026.
[20] S. Sarangapani, B.V. Tilak, C.P. Chen, J. Electrochem. Soc. 143 (1996) 3791.
[21] J.P. Zheng, P.J. Cygan, T.R. Jow, J. Electrochem. Soc. 142 (1995) 2699.
[22] J.P. Zheng, T.R. Jow, J. Electrochem. Soc. 142 (1995) L6.
[23] S.C. Pang, M.A. Anderson, T.W. Chapman, J. Electrochem. Soc. 147 (2000) 444.
[24] T. Moromoto, K. Hiratsuka, Y. Sanada, K. Kurihara, J. Power Sources 60 (1996) 239.
[25] D.C. Wu, X. Chen, S.H. Lu, Y.R. Liang, F. Xu, R.W. Fu, Micropor. Mesopor. Mater. 131 (2010) 261.
[26] C.H. Hou, C.D. Liang, S. Yiacoumi, S. Dai, C. Tsouris, J. Colloid Interface Sci. 302 (2006) 54.
[27] H. Zhou, D. Li, M. Hibino, I. Honma, Angew. Chem. Int. Ed. 44 (2005) 797.
[28] K.H. Chang, C.C. Hu, Appl. Phys. Lett. 88 (2006) 193, 102.
[29] C.C. Hu, K.H. Chang, M.C. Lin, Y.T. Wu, Nano Lett. 6 (2006) 2690.
[30] D.N. Futaba, K. Hata, T. Yamada, T. Hiraoka, Y. Hayamizu, Y. Kakudate, O. Tanaike, H. Hatori, M. Yumura, S. Iijima, Nat. Mater. 5 (2006) 987.
[31] Y. Hanzawa, H. Hatori, N. Yoshizawa, Y. Yamada, Carbon 40 (2002) 575.
[32] Z.L. Wang, X.B. Zhang, X.J. Liu, M.F. Lv, K.Y. Yang, J. Meng, Carbon 49 (2011) 161.
[33] R.W. Fu, T.F. Baumann, S. Cronin, G. Dresselhaus, M.S. Dresselhaus, J.H. Satcher Jr., Langmuir 21 (2005) 2647.
[34] R.W. Fu, M.S. Dresselhaus, G. Dresselhaus, B. Zheng, J. Liu, J.H. Satcher Jr., T.F. Baumann, J. Non-Cryst. Solids 318 (2003) 223.
[35] S.J. Kim, S.W. Hwang, S.H. Hyun, J. Mater. Sci. 40 (2005) 725.
[36] Z. Chen, V. Augustyn, J. Wen, Y.W. Zhang, M.Q. Shen, Adv. Mater. 23 (2011) 791.
[37] Y.J. Lee, J.C. Jung, S.Y. Park, J.G. Seo, S.H. Baeck, J.R. Yoon, J.H. Yi, I.K. Song, Curr. Appl. Phys. 10 (2010) 947.
[38] J. Li, X.Y. Wang, Y. Wang, Q.H. Huang, C.L. Dai, S. Gamboa, P.J. Sebastian, J. Non-Cryst. Solids 354 (2008) 19.
[39] R.W. Pekela, US Patent 4997804 (1991).
[40] F. Tuinstra, J.L. Koening, J. Chem. Phys. 53 (1970) 1126.
[41] E. Asari, M. Kitajima, K.G. Nakamura, Carbon 36 (1998) 1693.
[42] H.K. Lin, H.C. Chiu, H.C. Tsai, S.H. Chien, C.B. Wang, Catal. Lett. 88 (2003) 169.
[43] B. Fang, L. Binder, J. Phys. Chem. B 110 (2006) 7877.
[44] L. Wei, G. Yushin, J. Power Sources 196 (2011) 4072.
[45] C. Lin, J.A. Ritter, B.N. Popov, J. Electrochem. Soc. 146 (1999) 3639.
[46] Y.W. Zhu, S. Murali, M.D. Stoller, K.J. Ganesh, W.W. Cai, P.J. Ferreira, A. Pirkle, R.M. Wallace, K.A. Cychosz, M. Thommes, D. Su, E.A. Stach, R.S. Ruoff, Science 332 (2011) 1537.